

Optimization of the shape (and topology) of the initial conditions for diffusion parameter identification

Stefan Kindermann[†] and Štěpán Papáček[‡]

Abstract

The design of an experiment, e.g., the setting of initial conditions, strongly influences the accuracy of the whole process of determining model parameters from data. We impose a sensitivity-based approach for choosing optimal design variables and study the optimization of the shape (and topology) of the initial conditions for an inverse problem of a diffusion parameter identification. Our approach, although case independent, is illustrated at the FRAP (Fluorescence Recovery After Photobleaching) experimental technique. The core idea resides in the maximization of a sensitivity measure, which depends on a specific experimental setting of initial conditions. By a numerical optimization, we find an interesting pattern of increasingly complicated (with respect to connectivity) optimal initial shapes. The proposed modification of the FRAP experimental protocol is rather surprising but entirely realistic and the resulting enhancement of the parameter estimate accuracy is significant.

Keywords. FRAP, sensitivity analysis, optimal experimental design, parameter identification, diffusion

MSC. 65M32, 35R30, 49Q10

1 Introduction

The common practice of setting experimental conditions resides on trial-error method performed by experimentalists while the subsequent data processing is not always taken into account. It is not a rare case that large amount of data is routinely generated without a clear idea about further data processing. Here, we suggest to analyze simultaneously both the data (i.e., the processes hidden in data) and the experimental protocol, aiming to establish the link between experimental conditions and the accuracy of our results. The whole idea is presented in a simplified case study of Fluorescence Recovery After Photobleaching (FRAP) data processing. It serves as a paradigmatic example of the inverse problem of identifying the diffusion parameter from spatio-temporal concentration measurements.

²Corresponding author. E-mail: kindermann@indmath.uni-linz.ac.at. Industrial Mathematics Institute, University Linz, Altenbergerstr. 69, 4040 Linz, Austria.

³Institute of Complex Systems, University of South Bohemia in České Budějovice, FFPW USB, CENAKVA, Zámek 136, 373 33 Nové Hradky, Czech Republic.

FRAP is a classical method used to study the mobility of fluorescent molecules in membranes of the living cells [1]. The FRAP technique is based on measuring the fluorescence intensity, which is proportional to the non-bleached particles concentration in response to a high-intensity laser pulse. We suppose the laser pulse (the *bleach*) causes an irreversible loss in fluorescence of a certain amount of particles originally in the bleached area. The monitored region or the region of interest (ROI) where the data are measured is usually an Euclidean 2D domain containing the bleached area. After the bleach, the change in fluorescence intensity in a monitored region is observed due to the transport of fluorescent compounds from the area outside the bleach as well as bleached particles from the bleached region to originally non-bleached regions. In general, we observe both recovery and loss in fluorescence in different regions corresponding to FRAP or FLIP (Fluorescence Loss in Photobleaching), respectively [2, 3]. The natural question to be asked is: How does the bleach shape (and topology) influence the accuracy of resulting parameter estimates¹. Therefore, the main focus of this study concerns the searching for the optimal bleach shape (and its topology), or, from the more mathematical viewpoint, to optimize binary-valued initial conditions in a diffusion-parameter identification problem with respect to sensitivity.

The rest of this article is organized as follows: In Section 2 we provide the preliminaries for the further optimization problem formulation as well as the background information concerning the FRAP method. In Section 3 we rigorously formulate the optimization problem, evaluate the key term in the objective function and announce the Proposition 3.2, which allows to solve the problem efficiently. Section 4 provides two numerical results: (i) set of solutions (depending on the characteristic time of diffusion) for an optimal setting of the bleached region shape and topology when the bleach depth is the only constraint, and (ii) corresponding results as in (i) when the total bleach energy is restricted as well. The novelty and benefits of our approach as well as outlooks for further research are resumed in the final Section 5.

2 Preliminaries

2.1 Inverse problem of model parameter identification from FRAP data

Based on the spatio-temporal FRAP data, the so-called *effective diffusion coefficient* was estimated using a closed form model [4, 5, 6] in past decades. Nowadays, numerical simulations are preferred, cf. [7, 8, 9, 10, 11], mainly because there is no need for some unrealistic assumptions.

Further, we consider a normal Fickian diffusion problem with a *constant* diffusion coefficient $D > 0$. In the setup of this paper, we assume a sufficiently large domain such that we can treat diffusion in the free space \mathbb{R}^2 . In FRAP, the simplest governing equation for the spatio-temporal distribution of fluorescent particle concentration $u(x, t)$ is a diffusion equation without reaction term as

¹The problem is partially solved in our paper [9] where we use a relation similar to (9) assuring smaller confidence intervals of the parameter estimates for the higher values of a sensitivity measure.

follows:

$$\frac{\partial}{\partial t}u(x, t) = D\Delta u(x, t) \quad x \in \mathbb{R}^2, t \in [0, T], \quad (1)$$

$$u(x, 0) = u_0(x) \quad x \in \mathbb{R}^2. \quad (2)$$

The main issue in FRAP and related identification problems is to find the value of the diffusion coefficient D from spatio-temporal measurement of the concentration $u(x, t)$. As another simplification, we assume a spatially radially symmetric observation domain, that is, we consider the data

$$\begin{aligned} \text{data} &:= u(x, t) \quad x \in \Omega \times [0, T], \\ \Omega &= \{x \in \mathbb{R}^2 \mid \|x\| \leq R\}. \end{aligned} \quad (3)$$

Hence, the data are observed on a cylinder with radius R and height T . The parameters $R, T > 0$ are fixed for the further analysis and not subject of optimization. Although, in practice, it is often more convenient to consider a square spatial domain (i.e., an image), our cylindrical domain is a reasonable general model to indicate the most important conclusions in our further analysis.

The data (3) are insofar idealized as in experiments, they are given only at discrete points $u(x_i, t_i)$, $i, 1, \dots, N_{\text{data}}$. However, for simplicity and as it was done in [9], we assume a sufficiently dense set of data points (x_i, t_i) such that the model (3) is valid with reasonable accuracy and such that certain sums over the data points can be approximately well by the corresponding integrals over $\Omega \times [0, T]$; see [9].

The equations (1)–(2) and the data (3) are the basis for all the subsequent analysis, hence, although we mentioned FRAP as one important application, our results are of course applicable to other diffusion parameter identification problem which are governed by similar equations and data assimilation processes.

Based on the parameters R, T , it is convenient to introduce the following scaling of the space and time coordinates:

$$\begin{aligned} z &:= \frac{x}{R}, \quad \tau := \frac{t}{T}, \\ v(z, \tau) &:= u(zR, \tau t) \Leftrightarrow u(x, t) = v\left(\frac{x}{R}, \frac{t}{T}\right) \quad v_0(z) := u_0(zR). \end{aligned} \quad (4)$$

For later use we define a scaled version of the inverse of the diffusion coefficient²

$$\beta := \frac{R^2}{4TD}. \quad (5)$$

The scaled concentration v satisfies the equation

$$\frac{\partial}{\partial \tau}v(z, \tau) = \frac{TD}{R^2}\Delta v(z, \tau) = \frac{1}{4\beta}\Delta v(z, \tau) \quad z \in \mathbb{R}^2, \tau \in [0, 1], \quad (6)$$

$$v(z, 0) = v_0(z) = u_0(zR) \quad z \in \mathbb{R}^2. \quad (7)$$

In our case of constant coefficients and free-space diffusion in two dimensions, the solution to this problem can be expressed by means of the Green's function $G(x, t; y)$ for the heat equation.

$$u(x, t) = \int_{\mathbb{R}^2} G(x - y, tD)u_0(y)dy, \quad v(z, t) = \int_{\mathbb{R}^2} G(z - y, \frac{\tau}{4\beta})v_0(y)dy \quad (8)$$

²For the characteristic diffusion time $t_c = \frac{R^2}{4D}$, we have $\beta = \frac{t_c}{T}$.

with the well-known two-dimensional heat kernel

$$G(z, t) := \frac{1}{4\pi t} e^{-\frac{\|z\|^2}{4t}}.$$

2.2 Sensitivity of the output observation with respect to model parameter

Given the data as above, the diffusion coefficient D can be inferred by fitting the solution given in (8) to the data on $\Omega \times [0, T]$. Because of unavoidable noise in the data, one obtains an estimated value \bar{D} which reasonably well approximates the true D . It can be shown, see [9, 12] and references within there, that for our case of single scalar parameter estimation and assuming white noise as data error, the expected relative error in D depends on the data noise and a factor, which we call relative global sensitivity S_{GRS} , as follows:

$$\mathbb{E} \left(\left| \frac{\bar{D} - D}{D} \right|^2 \right) \sim \frac{1}{S_{GRS}} \frac{\sigma^2}{u_{\text{ref}}^2}, \quad (9)$$

where σ^2 denotes the noise variance (and $\frac{\sigma}{u_{\text{ref}}}$ is related to the coefficient of variation or to the inverse of the signal to noise ratio), and u_{ref} is some (chosen) reference value of the observed output.

The global relative squared sensitivity is given by

$$S_{GRS} := \frac{D^2}{u_{\text{ref}}^2} \sum_{i=1}^{N_{\text{data}}} \left(\frac{\partial}{\partial D} u(x_i, t_i) \right)^2, \quad (10)$$

where $\frac{\partial u}{\partial D}(x_i, t_i)$ is the usual sensitivity of the output observation data point (x_i, t_i) with respect to the parameter D and N_{data} is the number of data points in space-time domain. It is obvious from this estimate that if the noise level is fixed, the estimation can be only improved by switching to an experimental design with a higher sensitivity. Thus, the thrive for good estimators \bar{D} leads to the problem of experimental design optimization in order to maximize the sensitivity measure S_{GRS} . The solution of this optimization problem, which is the central aspect of this article, is rigorously formulated and partially solved in the next Section 3.

3 Optimization of the bleach design

3.1 Problem formulation

The sensitivity measure (10) involves several design parameters. Note that R and T are involved implicitly because the number of data points $N_{\text{data}} \approx \frac{\pi R^2 T}{\Delta x \Delta t}$, where Δx is defined by the pixel size and Δt corresponds to the time interval between two consecutive measurements. However, if all the above parameters $R, T, \Delta x, \Delta t$ are fixed, there is only one way to maximize the sensitivity measure S_{GRS} : considering the *initial bleach* u_0 in (2) as the experimental design parameter. By optimizing the bleach design, we mean to select the initial conditions in such a way that S_{GRS} is maximized and hence the expected error in D minimized. In order to do so, we have to chose the class of designs out of which

we take the initial conditions. In FRAP, it is the usual case that the initial bleach u_0 is a binary-valued function with fixed given values $u_0(x) \in \{u_{00}, 0\}$, $u_{00} > 0$. Without loss of generality, we assume $u_0(x)$ being a $\{1, 0\}$ -function, which also cancels out the term u_{ref} in S_{GRS} ³:

$$u_0(x) = \begin{cases} 1 & x \in B \\ 0, & \text{else,} \end{cases}$$

with some bounded open set B , the *bleach shape*. Moreover, if the sum in the term S_{GRS} is furthermore approximated by an integral

$$\sum_{i=1}^{N_{data}} \left(\frac{\partial}{\partial D} u(x_i, t_i) \right)^2 \sim \frac{N_{data}}{\pi R^2 T} \int_{\|x\| \leq R} \int_0^T \left| \frac{\partial}{\partial D} u(x, t) \right|^2 dx dt,$$

then we have a final sensitivity term S_{int} to be maximized:

$$S_{int} := \int_{\|x\| \leq R} \int_0^T \left| \frac{\partial u}{\partial D}(x, t) \right|^2 dx dt. \quad (11)$$

Depending on the different restrictions imposed on the initial bleach, we study the following two setups:

- Problem 1: optimization with fixed bleach depth

$$S_{int} \rightarrow \max_{B \subset \mathbb{R}^2} \quad \text{with} \quad u_0(x) = \begin{cases} 1 & x \in B \\ 0 & \text{else} \end{cases},$$

over the set of bounded open sets $B \subset \mathbb{R}^2$.

- Problem 2: optimization with fixed bleach depth and fixed energy

$$S_{int} \rightarrow \max_{B \subset \mathbb{R}^2} \quad \text{with} \quad u_0(x) = \begin{cases} 1 & x \in B \\ 0 & \text{else} \end{cases} \quad \text{and} \quad \int_{\mathbb{R}^2} u_0(x) dx = c_1,$$

$c_1 > 0$ given, over the set of bounded open sets $B \subset \mathbb{R}^2$.

Note that these problems are shape (and topology) optimization problems, i.e., the unknown bleach shape B is the independent variable.

However, the problems can be simplified by restricting B to a radially symmetric shapes; the reason for that is the following lemma.

Lemma 3.1 *If solutions to the Problems 1 and 2 exists, then there also exists radially symmetric solutions. In particular, if the solutions are unique, they must be radially symmetric.*

Proof: It is easy to see that the sensitivity measure S_{int} is a convex functional of the initial conditions. From convex analysis, we conclude that the optimization problems can be relaxed and expressed as problems with box constraints. In either case, the set of initial conditions can be relaxed to

$$u_0 \in \{w(x) \mid 0 \leq w(x) \leq 1\}, \quad (12)$$

³When we choose $u_{\text{ref}} = u_{00}$, then the normalization of the signal, i.e. $0 \leq u(x) \leq 1$ is actually done due to the division by the maximal value which signal u can reach, cf. (10).

without altering the solution. Indeed, this holds because a convex functional attains its maximum at the boundary, hence, by considering the relaxed constraints (12), a solution will be at the boundary of the admissible domain in (12) and hence a $\{0, 1\}$ -function. Thus, solutions of the relaxed problem are also solutions of the original problem (and vice versa).

Due to our choice of an observation domain, the problem is invariant with respect to coordinate rotations, i.e., the sensitivity does not change if the initial bleach is rotated. If $u_0(x)$ is a solution to the optimization problem, then so is $u_0(Q_\theta x)$ for any rotation Q_θ around the origin with angle θ . It is easy to see that taking the angle-averaged initial condition $\frac{1}{2\pi} \int_0^{2\pi} u_0(Q_\theta z) d\theta$ yields a solution to the relaxed optimization problem which is radially symmetric. Because it must also be a solution to the original problem, the set B must be radially symmetric. ■

Note that Lemma 3.1 is not valid if the observation domain is not radially symmetric. When speaking to experimentalists, the result of Lemma 3.1 is usually intuitively clear to them. However, a first guess for the optimal shape that is often uttered by them, is that it must be a “disk” (or a ball). It is maybe the main conclusion of our work that this guess not always hits the truth as the optimal shape can be an annulus or multiple annuli as well; see below.

Remark 3.2 Let us mention several related design optimization problems. In a previous paper [9], the authors have considered the problem of optimizing the sensitivity with respect to the observation domain R, T and also the problem of selecting reduced data that only little reduce the sensitivity S_{GRS} .

In view of the initial conditions, there are other classes of designs possible, for instance, if not binary-valued functions are used, then it is natural to optimize sensitivity with respect to a fixed energy (i.e., the L^1 -norm) of the initial conditions. That is, the problem

$$S_{int} \rightarrow \max_{u_0} \quad \text{with} \quad \int_{\mathbb{R}^2} u_0(x) dx = c_1$$

with $c_1 > 0$ given. However, when analyzing this problem, one finds out that it does not have a solution. A sequence of almost optimal solutions will tend to a δ -distribution. Thus a δ -peak is the “optimal” solution in this case. The sensitivity is infinite for this case, which is caused by the fact that the solutions are not square-integrable any more. Thus, for a δ -peak, one cannot use the formula above for the expected error but have to use different, weighted norms (for the data noise and the sensitivity).

A similar problem is that one with a fixed L^2 -norm.

$$S_{int} \rightarrow \max_{u_0} \quad \text{with} \quad \int_{\mathbb{R}^2} u_0(x)^2 dx = c_2$$

This one has an appealing interpretation as eigenvalue problem: indeed, let K be the linear operator $L^2(\mathbb{R}^2) \rightarrow L^2(\Omega \times [0, T])$ that maps the initial conditions to $\frac{\partial u}{\partial D}$ on the observation domain. It can be shown that this is a bounded linear and compact operator. The problem can be rephrased in functional analytic language as

$$\|K u_0\|_{L^2(\Omega \times [0, T])}^2 \rightarrow \max \quad \text{with} \quad \|u_0\|_{L^2(\mathbb{R}^2)} \leq c_2.$$

It is well known that a solution exists and it is given by the right singular function associated to the largest singular value of K . The associated optimization problem thus can be (approximately) solved by applying a standard singular valued decomposition to the discretized operator K .

Going back to the optimization problems, Problems 1 and 2, it can be observed that the sensitivity S_{int} is a quadratic functional with respect to u_0 . For the optimization it is important to have an efficient formula for S_{int} available, since it has to be evaluated many times (for different initial conditions). Solving the PDE (1)–(2) is not convenient in that respect. We rather stick to the integral representation by the Green's function and derive a formula for the sensitivity S_{int} in the next section.

3.2 Evaluating the sensitivity measure (11)

The formula for S_{int} involves the derivative of the observation $u(x, t)$ with respect to the diffusion parameter D . Either by differentiating (1)–(2) or (8), we find that

$$\frac{\partial u}{\partial D}(x, t) = \frac{t}{D} \frac{\partial}{\partial t} u(x, t) = t \Delta u(x, t) = t \Delta_x \int_{\mathbb{R}^2} G(x - y, tD) u_0(y) dy.$$

Because a convolution integral commutes with differentiation, we also find that

$$\frac{\partial u}{\partial D}(x, t) = t \int_{\mathbb{R}^2} G(x - y, tD) \Delta u_0(y) dy.$$

In a similar way, we can derive a formula using the scaled variables:

$$\frac{\partial u}{\partial D}(zR, \tau T) = \frac{T}{R^2} \tau \int_{\mathbb{R}^2} G(z - y, \frac{\tau}{4\beta}) \Delta v_0(y) dy = \frac{T}{R^2} \tau \Delta v(z, \tau) \quad (13)$$

with $v_0(y) = u_0(Ry)$.

Now, in order to solve the above optimization problems (Problems 1 and 2), we have to evaluate (10) for many different initial conditions. Therefore, in the sequel we derive the kernel of the quadratic form associated to the sensitivity measure S_{int} .

Consider two solutions $u^{(1)}$ and $u^{(2)}$ of (1)–(2) with the respective initial conditions $u_0^{(1)}$ and $u_0^{(2)}$. We associate to them the scaled functions $v^{(1)}$ and $v^{(2)}$ as in (4). We calculate the following pairing of $u^{(1)}$ and $u^{(2)}$:

$$\begin{aligned} & \int_{\|x\| \leq R} \int_0^T \frac{\partial u^{(1)}}{\partial D}(x, t) \frac{\partial u^{(2)}}{\partial D}(x, t) dx dt \\ &= TR^2 \int_{\|z\| \leq 1} \int_0^1 \frac{\partial u^{(1)}}{\partial D}(zR, \tau T) \frac{\partial u^{(2)}}{\partial D}(zR, \tau T) dz d\tau \\ &= TR^2 \int_{\|z\| \leq 1} \int_0^1 \tau^2 \Delta v^{(1)}(z, \tau) \Delta v^{(2)}(z, \tau) dz d\tau \\ &= \frac{T^3}{R^2} \int_{\|z\| \leq 1} \int_0^1 \int_{\mathbb{R}^n} \int_{\mathbb{R}^n} \tau^2 G(z - y, \frac{\tau}{4\beta}) G(z - w, \frac{\tau}{4\beta}) \Delta v_0^{(1)}(y) \Delta v_0^{(2)}(w) dw dy d\tau dz \\ &= \frac{T^3}{R^2} \frac{\beta^2}{\pi^2} \int_{\|z\| \leq 1} \int_0^1 \int_{\mathbb{R}^n} \int_{\mathbb{R}^n} e^{-\beta \frac{\|z-y\|^2 + \|z-w\|^2}{\tau}} \Delta v_0^{(1)}(y) \Delta v_0^{(2)}(w) dw dy d\tau dz. \end{aligned}$$

In the next step we assume radially symmetric initial conditions and introduce polar coordinates:

$$y = r(\cos(\theta_1), \sin(\theta_1)) \quad w = s(\cos(\theta_2), \sin(\theta_2)) \quad z = q(\cos(\phi), \sin(\phi))$$

$$v_0^{(1)}(y) =: g^{(1)}(\|y\|) = g^{(1)}(r) \quad v_0^{(2)}(w) =: g^{(2)}(\|w\|) = g^{(2)}(s)$$

such that

$$\Delta v_0^{(1)}(y) = \frac{1}{r} \frac{\partial}{\partial r} \left(r \frac{\partial}{\partial r} g^{(1)}(r) \right) \quad r = \|y\|,$$

$$\Delta v_0^{(2)}(w) = \frac{1}{s} \frac{\partial}{\partial s} \left(s \frac{\partial}{\partial s} g^{(2)}(s) \right) \quad s = \|w\|.$$

Thus,

$$\begin{aligned} & \int_{\|x\| \leq R} \int_0^T \frac{\partial u^{(1)}}{\partial D}(x, t) \frac{\partial u^{(2)}}{\partial D}(x, t) dx dt \\ &= \frac{T^3}{R^2} \frac{\beta^2}{\pi^2} \int_0^1 q \int_0^1 \int_{\mathbb{R}} \int_{\mathbb{R}} \int_0^{2\pi} \int_0^{2\pi} \int_0^{2\pi} e^{-\frac{\beta}{\tau}(q^2+r^2-2qr \cos(\phi-\theta_1)+q^2+s^2-2qs \cos(\phi-\theta_2))} \\ & \quad r s \frac{1}{r} \frac{\partial}{\partial r} \left(r \frac{\partial}{\partial r} g^{(1)}(r) \right) \frac{1}{s} \frac{\partial}{\partial s} \left(s \frac{\partial}{\partial s} g^{(2)}(s) \right) d\theta_1 d\theta_2 d\phi dr ds d\tau dq. \end{aligned}$$

By a substitution of $\phi - \theta_1$ by θ_1 and $\phi - \theta_2$ by θ_2 , the integrand does not depend on ϕ . Thus, the corresponding integral gives a contribution of 2π . The integrals over θ_i can be calculated explicitly using the formula

$$\int_0^{2\pi} e^{a \cos(t)} dt = 2\pi I_0(a), \quad (14)$$

with the modified Bessel function $I_k(z)$.

$$\begin{aligned} & \int_{\|x\| \leq R} \int_0^T \frac{\partial u^{(1)}}{\partial D}(x, t) \frac{\partial u^{(2)}}{\partial D}(x, t) dx dt \\ &= \frac{T^3}{R^2} 8\pi \beta^2 \int_0^1 q \int_0^1 \int_{\mathbb{R}} \int_{\mathbb{R}} e^{-\frac{\beta}{\tau}(q^2+r^2+q^2+s^2)} I_0\left(\frac{2\beta qr}{\tau}\right) I_0\left(\frac{2\beta qs}{\tau}\right) \\ & \quad \frac{\partial}{\partial r} \left(r \frac{\partial}{\partial r} g^{(1)}(r) \right) \frac{\partial}{\partial s} \left(s \frac{\partial}{\partial s} g^{(2)}(s) \right) d\theta_1 d\theta_2 dr ds d\tau dq. \end{aligned}$$

We next assume that $g^{(1)}$ and $g^{(2)}$ have compact support and we integrate by parts with respect to the derivatives $\frac{\partial}{\partial r}$ and $\frac{\partial}{\partial s}$ observing that by radial symmetry the terms at $r = 0$ and $s = 0$ vanish. Thus,

$$\begin{aligned} & \int_{\|x\| \leq R} \int_0^T \frac{\partial u^{(1)}}{\partial D}(x, t) \frac{\partial u^{(2)}}{\partial D}(x, t) dx dt \\ &= \frac{T^3}{R^2} 8\pi \beta^2 \int_0^1 q \int_0^1 \int_{\mathbb{R}} \int_{\mathbb{R}} \frac{\partial^2}{\partial r \partial s} \left[e^{-\frac{\beta}{\tau}(q^2+r^2+q^2+s^2)} I_0\left(\frac{2\beta qr}{\tau}\right) I_0\left(\frac{2\beta qs}{\tau}\right) \right] \\ & \quad r s \frac{\partial}{\partial r} g^{(1)}(r) \frac{\partial}{\partial s} g^{(2)}(s) dr ds d\tau dq. \end{aligned}$$

The r, s -derivatives can be calculated using the fact for modified Bessel functions that $I'_0 = I_1$.

$$\begin{aligned} & \frac{\partial^2}{\partial r \partial s} \left[e^{-\frac{\beta}{\tau}(q^2+r^2+q^2+s^2)} I_0\left(\frac{2\beta qr}{\tau}\right) I_0\left(\frac{2\beta qs}{\tau}\right) \right] \\ &= e^{-\frac{\beta}{\tau}(q^2+r^2+q^2+s^2)} \times \\ & \quad \left\{ \frac{-2r\beta}{\tau} I_0\left(\frac{2\beta qr}{\tau}\right) + \frac{2q\beta}{\tau} I_1\left(\frac{2\beta qr}{\tau}\right) \right\} \left\{ \frac{-2s\beta}{\tau} I_0\left(\frac{2\beta qs}{\tau}\right) + \frac{2q\beta}{\tau} I_1\left(\frac{2\beta qs}{\tau}\right) \right\}, \end{aligned}$$

which with $\rho = \frac{\beta}{\tau}$ finally leads to

$$\begin{aligned} & \int_{\|x\| \leq R} \int_0^T \frac{\partial u^{(1)}}{\partial D}(x, t) \frac{\partial u^{(2)}}{\partial D}(x, t) dx dt \\ &= \frac{T^3}{R^2} 32\pi\beta^3 \int_0^1 q \int_{\beta}^{\infty} \int_{\mathbb{R}} \int_{\mathbb{R}} e^{-\rho(q^2+r^2+q^2+s^2)} \times \\ & \quad \{rI_0(2qr\rho) - qI_1(2qr\rho)\} \{sI_0(2qs\rho) - qI_1(2qs\rho)\} \\ & \quad rs \frac{\partial}{\partial r} g^{(1)}(r) \frac{\partial}{\partial s} g^{(2)}(s) dr ds dp dq. \end{aligned} \tag{15}$$

For later reference we define a kernel as follows:

$$\begin{aligned} k(r, s) &:= \int_0^1 q \int_{\beta}^{\infty} e^{-\rho(q^2+r^2+q^2+s^2)} \times \\ & \quad \{rI_0(2qr\rho) - qI_1(2qr\rho)\} \{sI_0(2qs\rho) - qI_1(2qs\rho)\} r s dp dq. \end{aligned} \tag{16}$$

For the numerical calculations, we also require the kernel for the case of $\beta = 0$. We present another formula which avoids integration over the infinite domain with respect to ρ .

Lemma 3.3 *For $\beta = 0$ the kernel $k(r, s)$ can be written as*

$$\begin{aligned} k(r, s) &= \\ & \frac{1}{4\pi^2} \int_0^1 \int_0^{2\pi} \int_0^{2\pi} q r s \frac{(r - q \cos(\theta_1)) (s - q \cos(\theta_2))}{q^2 + r^2 - 2qr \cos(\theta_1) + q^2 + s^2 - 2qs \cos(\theta_2)} d\theta_1 d\theta_2 dq \end{aligned} \tag{17}$$

Proof: Setting $\beta = 0$ and (14) and

$$I_1(a) = \frac{1}{2\pi} \int_0^{2\pi} e^{a \cos(\theta)} \cos(\theta) d\theta,$$

we observe that

$$\begin{aligned} k(r, s) &= \frac{1}{4\pi^2} \int_0^1 q \int_0^{2\pi} \int_0^{2\pi} e^{-\rho(q^2+r^2-2qr \cos(\theta_1)+q^2+s^2-2qs \cos(\theta_2))} \times \\ & \quad (r - q \cos(\theta_1)) (s - q \cos(\theta_2)) r s d\theta_1 d\theta_2 dp dq \\ &= \frac{1}{4\pi^2} \int_0^1 \int_0^{2\pi} \int_0^{2\pi} q r s \frac{(r - q \cos(\theta_1)) (s - q \cos(\theta_2))}{q^2 + r^2 - 2qr \cos(\theta_1) + q^2 + s^2 - 2qs \cos(\theta_2)} d\theta_1 d\theta_2 dq. \end{aligned}$$

■

Next we use Lemma 3.1 according to which the optimal initial conditions are radially symmetric $\{0, 1\}$ -valued with compact support. This means that in this case, the functions $g^{(i)}$ attain the value 1 on a number of intervals and 0 else, and the associated initial condition is supported on a union of annuli and possibly a disk. We moreover assume that the function g , which defines the initial conditions, has only jumps at $N \in \mathbb{N}$ places:

$$g^{(i)}(r) = \begin{cases} 1 & r \in [r_j, r_{j+1}], j = 1, \dots, N, 0 \leq r_1 < r_{j-1} < r_j < r_{j-1}, \\ 0 & \text{else} \end{cases} \quad (18)$$

It follows in the sense of distributions that

$$\frac{\partial}{\partial r} g^{(i)}(r) = \sum_{j=1, r_1 \neq 0}^N (-1)^{N-j+1} \delta_{r_j}(r), \quad (19)$$

where δ denotes the Dirac-distribution. The case that $r_1 = 0$ means that u_0 has support in a disk around 0 and clearly, there is no jump in the derivative there, hence this must be excluded from the sum. Note that the signs are such that the outer radius has (-1) and the following have alternating signs, which becomes clear by drawing the graph of such a function.

By plugging in the formula (19) in place of $g^{(i)}$ we obtain the following proposition.

Proposition 3.4 *Suppose that the initial conditions $v_0(z) = g(|z|)$ are radially symmetric $\{0, 1\}$ -valued with g having finitely many jumps as in (18). Then the sensitivity is given by*

$$S_{int} = \frac{T^3}{R^2} 32\pi\beta^3 \sum_{j,k=1}^N (-1)^{k+j} k(r_j, r_k) \quad (20)$$

with the kernel k given by (16).

Note that we do not have to take into account if $r_1 = 0$ or not, because the kernel is 0 if one of the arguments is 0. We remark that Proposition 3.4 is also true for the case of g having infinitely many jumps; in this case we have to set $N = \infty$.

By Proposition 3.4 we find that

- Problem 1 is equivalent to

$$\max_{r_i, N} \sum_{j,k=1}^N (-1)^{k+j} k(r_j, r_k), \quad 0 < r_1 < r_2 \leq \dots r_N, N \geq 1.$$

- Problem 2 is equivalent to

$$\max_{r_i, N} \sum_{j,k=1}^N (-1)^{k+j} k(r_j, r_k), \quad 0 < r_1 < r_1 \leq \dots r_N, N \geq 1$$

under the constraint that

$$\sum_{k=N}^2 r_k^2 - r_{k-1}^2 = \frac{c_1}{\pi} \quad \text{or} \quad r_1^2 = \frac{c_1}{\pi} \quad \text{if } N = 1.$$

3.3 Shape (and topology) optimization of the bleached region

We try to solve the above problems numerically. Note that we have the radii of the annuli/disks as variables and the number N of them. As optimization routine we use the simplest and least sophisticated one, namely grid search over the radii restricting us to a finite number of annuli. In fact, we managed to search for the case $N \leq 4$ and for radii restricted to $r_i \leq 5$ on a sufficiently fine grid. We could not think of a smarter algorithm, but there are good reasons to believe that there is no fast algorithm available. In fact, by considering the relaxed problem and introducing the initial-to-sensitivity operator K , Problem 1 is equivalent to

$$\|Ku_0\|_{L^2(\Omega) \times [0, T]}^2 \rightarrow \max \quad \text{under } 0 \leq u_0 \leq 1.$$

This is a convex *maximization problem* and it can be regarded as the problem of calculating the operator norm $K : L^\infty \rightarrow L^2$ (together with an additional positivity constraint $u_0 \geq 0$). It is known that calculating this operator norm is an NP-hard problem [13, 14]. This makes us believe that our optimization problems are hard problems indeed and that there is no simple efficient algorithm possible.

Let us mention that a classical method to tackle such shape optimization methods is the *level set method* [15]. This could be applied as well here, but the problem is that this and related methods can only find *local* maxima. Thus, as we want to find *global* maxima, the level set method does not help much here.

4 Numerical calculations and results

As mentioned in Section 3.3, we perform a grid search to solve Problems 1 and 2. For this we have to calculate the kernel $k(r, s)$ for different values of r and s and also, to understand the parameter dependence of the results, for different values of β . The results are calculated using Matlab. Depending on the grid for r, s , and β , according to (16), we have to calculate a double integral for each point on a 3-dimensional grid on (r, s, β) . No doubt, that for this tasks the evaluation has to be done efficiently in order to have a reasonable runtime. When calculating the double integral in (16), we observe that Matlab does not have an ‘‘ArrayValued’’ option for multidimensional integrals and hence the code cannot be vectorized. This faces us with the problem that the 2-dimensional integral has to be calculated by for-loops over the grid, which, as is well-known, is usually extremely slow. As a remedy, we rewrite the problem as iterated integral and apply Matlab’s ODE-solver (which can be vectorized).

Indeed, from formula (16), it follows that the kernel satisfies

$$\begin{aligned} \frac{\partial}{\partial \beta} k(r, s) = & - \int_0^1 q e^{-\rho(q^2+r^2+q^2+s^2)} \times \\ & \{rI_0(2qr\rho) - qI_1(2qr\rho)\} \{sI_0(2qs\rho) - qI_1(2qs\rho)\} r s dq. \end{aligned} \tag{21}$$

with initial condition

$$k(r, s)|_{\beta=0} = (17)$$

In this way we can use the ODE-solver to handle the β -dependence and only have to calculate the one-dimensional parameter-dependent integral (21), where both steps can be vectorized. This gives a speed-up of a factor of about 10 compared to the for-loop and double integral approach. The only bottleneck is the calculation of the initial conditions in form of a 3-dimensional integral. However, this only has to be done on a 2-dimensional (r, s) parameter grid (compared to the initially 3-dimensional parameter domain including β).

4.1 Problem 1

We try to calculate the (numerically) optimal configuration for Problem 1. As explained above, we only have to consider radially symmetric initial conditions. We cannot calculate all configurations but we restrict us to the case of at most $N = 4$ radii. This means we consider initial shapes in the form of a disk ($N = 1$), an annulus ($N = 2$), an annulus with a disk inside ($N = 3$), or a double annulus ($N = 4$). Other configurations with higher N are excluded because of runtime considerations. However, the solutions indicate a pattern, which makes us believe that we have found the optimal configurations in the respective parameter setting of β .

We also note that we only have to evaluate the kernel k because the sensitivity is only multiplied by a constant which only depends on the parameters R, T, D . Thus, with these values fixed, optimizing k is the same as optimizing S_{int} .

Let us come to the details of our calculations: We set up a grid for r and s in the interval $[0, 5]$ with 100 equal-sized subintervals (of length 0.05). For β we set up a grid in the interval $[0, 20]$ with 200 subintervals of length 0.1. Then the kernel is calculated on these gridpoints (exploiting symmetry in r and s). With the calculated kernel, we evaluate the functional for r, s on the grid for Problem 1 as given in Proposition 3.4 for the cases $N = 1, 2, 3, 4$ and find the configuration that has maximal value. Note that this testing requires up to 4 for-loops and is thus quite slow. The results are depicted in Figure 1.

Let us explain the figure. The x-axis indicates the values of β while the y-axis corresponds to the logarithm of the optimal value of the sensitivity for a fixed β . The full lines in the figure display the log of the optimal value over β and the associated colors encode which of the four possibilities ($N = 1, \dots, 4$) are the optimal configuration (violet: $N = 1$, green: $N = 2$, blue: $N = 3$, red: $N = 4$).

It can be observed that there are clear intervals for β where one specific configuration is always optimal. A value of β where the shape of the optimal configuration changes (e.g., from disk to annulus) is indicated by a vertical line. Thus, we observe that from $\beta \in [0, 1.8]$ the disk ($N = 1$) is the optimal configuration, whereas for higher β in the interval $[1.8, 6.1]$ the annulus is optimal. An even higher β gives an annulus with a disk inside and for $\beta > 13.8$ we find the double annulus as optimal. Clearly a pattern can be observed, namely that for increasing β the number of components of the optimal shape increases. We expect that for higher β not in the range of our calculations, more complicated shapes (e.g. with $N = 5$) are optimal. Although we tested only to $N = 4$ the given pattern indicates that in the low range of β , the shapes with few components are indeed optimal because in the first interval $\beta \in [0, 1.8]$ we never found a better structure with $N > 1$.

In Figure 1 we also indicated the log-values of the optimal sensitivity for each shape with fixed N by a dotted line. For instance, the dotted continuation of the violet line from $\beta = 1.8$ on corresponds to the optimal value within all disks (i.e. $N = 1$.) The continuation of the green line corresponds to the optimal value within all annuli and so on. It can be observed that, for instance, in the range where the annulus is optimal, the value of the sensitivity is significantly higher than the best disk. Roughly, the sensitivity of the best annulus is about twice that of the best disk. This indicates that in practice and for certain parameter setups, there can be a significant gain of confidence when using an annulus instead of a disk as initial bleach.

In the second figure, Figure 2, we plotted the values of the radii of the optimal configuration in each interval of β . On the x-axis we put again the value of β and on the y-axis we have the scaled radius. For instance in $\beta \in [0, 1.8]$ the disk is optimal and only one radius is required for its parameterization. The value of the optimal radius is given by the curve in the interval $[0, 1.8]$ In the next interval, the annulus is optimal which has an outer and an inner radius as given by the two curves and so on, up to the double annulus with 4 radii. Note that the jumps in this graphs inside of the intervals are artefacts due to the discrete grid for the radius; the exact curves should be smooth.

In Figure 3, we plotted the energy (i.e., the L^1 -norm $\int_{\mathbb{R}^2} u_0(x) dx$) of the optimal configurations as in Figure 2. Of course, those can be easily calculated from the radii in Figure 2.

For illustration purposes, in Figure 4 we present some optimal initial shapes for some representative values of β in each of the intervals, for $\beta = 1, 3, 10, 18$ (from left to right, from top to bottom).

4.2 Problem 2

The results from Problem 1 can also be used for Problem 2. Here we have the additional restriction on the energy. The energy of some optimal configurations without constraints can be read off from Figure 3.

In order to find an optimal shape, we again restrict ourselves to $N \leq 4$. We calculate the value of the kernel for different configurations, i.e., values of N , and r_i and additionally calculate their energy (the area of the initial bleach shape in this case). For each of the four cases of N we pick the configuration which is optimal for each energy. Note that this comes with a slight difficulty because due to the discretization of the radii, the energy values are discrete and in order to compare configurations, we have to interpolate these values to a common energy grid. Note that for the case $N = 1$, when fixing the energy, the disk is uniquely determined by the energy and there is no need to optimize in this case because no degree of freedom is left.

In Figure 4.2, we display again a color-coded plot indicating the optimal configurations (up to $N \leq 4$). For each value of the energy and each value of β , the color at the corresponding pixel indicates which of the configurations are found optimal. We observe that in the majority of cases the double annulus is optimal, but this is only because we restricted ourselves to $N \leq 4$. It is to be expected that initial shapes with more annuli are optimal in general and the problem does not reveal an obvious pattern. Furthermore, we observe that the plot has quite irregular regions with not always clearly defined boundaries. This

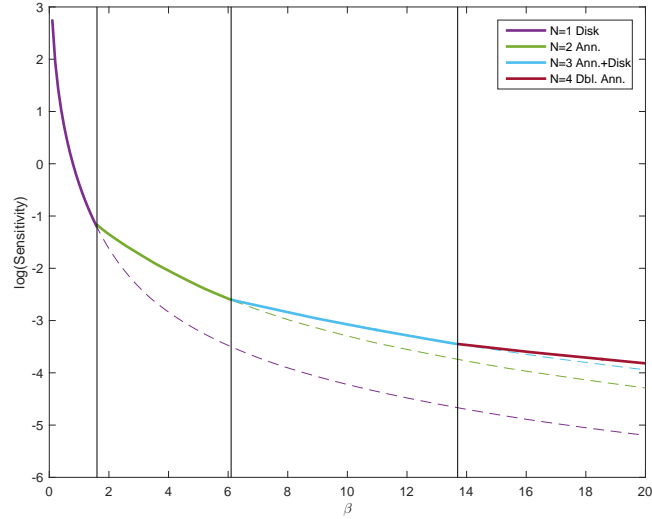


Figure 1: Optimal configurations for different values of β . Tested were all configurations with $N \leq 4$. Thick lines: values of the log of the optimal sensitivity. Dashed lines: values of the log of the optimal sensitivity within each configurations (e.g. $N = 1, N = 2, N = 3$).

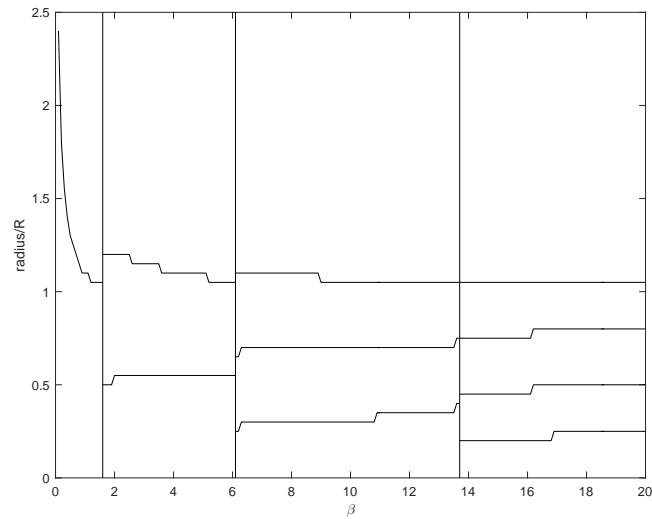


Figure 2: Scaled radii of the optimal configurations as a function of β .

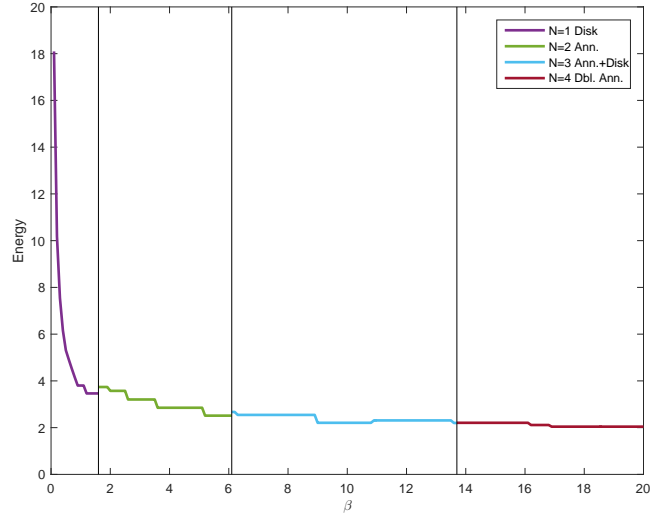


Figure 3: Energy (i.e., $\int_{\mathbb{R}^2} u_0(x) dx$) of the optimal configurations as a function of β .

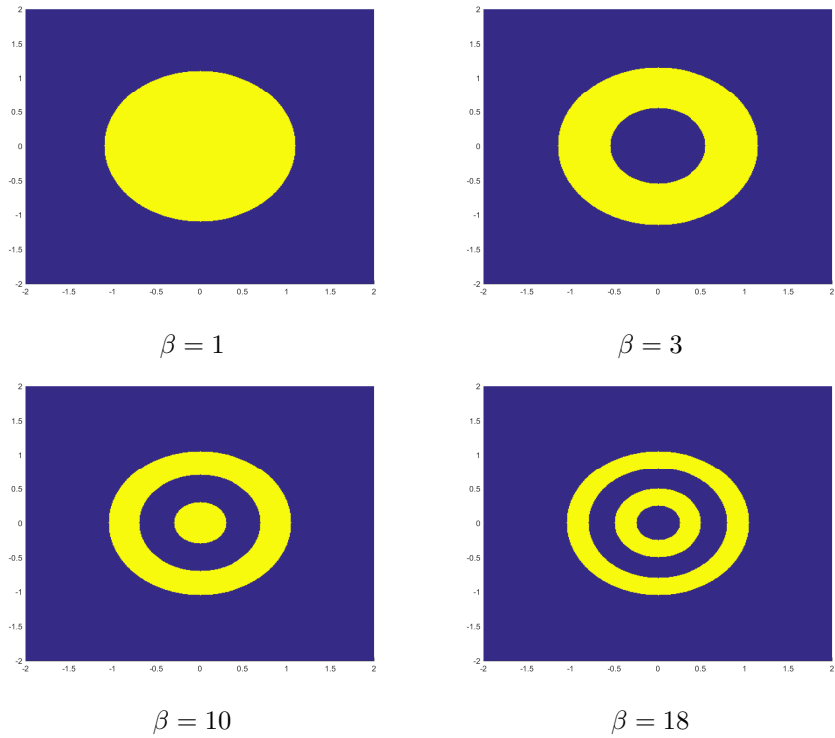


Figure 4: Optimal shapes of initial bleach for various values of β .

can be an artefact of the discretization and we consider the plot only as rough indication of what is going on.

Only in a tiny region around $\beta \sim 0$ energy ~ 2 , we have a situation where the disk is optimal, but it is uncertain if this is a valid result or an artefact from our discretization and the interpolation of the energy values. As a summary, it is quite likely that simple-shaped objects (i.e., those with small N) are rarely (or even never) optimal for Problem 2.

Although, we have put some model assumptions like symmetric observation domain and simple diffusion with constant parameter, we think that our results are relevant and—with modification—valid also in more general cases. In particular, when the observational domain is not a disk but a square, we expect the optimal bleach shape for Problem 1 being a rounded square or several nested rounded squares, where the connectivity again increases with β . For non-constant diffusion, the sensitivity is represented by a matrix and the optimal experimental design leads to the problem of maximizing some matrix norm of the inverse of the Fisher information matrix. Then, the optimal bleach shape for Problem 1 might depend on several additional design setups like the basis representation of the diffusion coefficient. Still it is not unlikely, that even in this case a similar pattern of optimal shapes with increasing connectivity emerges.

5 Conclusion

Our study started with the question: How does the bleach shape (and topology) influence the accuracy of resulting parameter estimates? Then the problem of the optimal initial shape for the identification of a constant diffusion parameter was formulated. As optimality criterion we choose to maximize a sensitivity measure in order to have the expected error minimal; cf. (10). We studied two problems, the first with the fixed bleach depth and the second with an fixed energy as an additional restriction. We found out the analytical expressions for the sensitivity measure S_{int} , cf. Proposition 3.2, allowing to compare different initial bleach shapes. Our numerical calculations revealed rather surprising results. For the first problem without restriction on energy, a clear pattern is revealed. For small values of the scaled inverse diffusion coefficient, the disk is the optimal shape and for higher values, shapes with more and more components (i.e. annuli-type shapes) become optimal. In particular, the disk is not always the best shape. For practically relevant values of the parameters, sometimes an annulus can be better leading to a significant improvement in the confidence intervals. For the later problem with restriction on energy, it seems to have in most of the cases or even always only highly oscillating solutions. However, our ongoing research is directed to this problem.

Acknowledgement

This work was supported by the Ministry of Education, Youth and Sports of the Czech Republic – projects CENAKVA (No. CZ.1.05/2.1.00/01.0024), the Cenakva Centre Development CZ.1.05/2.1.00/19.0380, and by the OeAD (Austrian agency for international mobility and cooperation in education, science and research) within the programme "Aktion Oesterreich-Tschechien (AOeCZ-Universitaetslehrerstipendien)".

References

- [1] Mueller, F., Mazza, D., Stasevich, T.J., McNally, J.G.: FRAP and kinetic modeling in the analysis of nuclear protein dynamics: what do we really know? *Current Opinion in Cell Biology* 22, 1–9 (2010)
- [2] Kaňa, R., Kotabová, E., Lukeš, M., Papáček, Š., Matonoha, C., Liu, L.N., Prášil, O., Mullineaux, C.W.: Phycobilisome mobility and its role in the regulation of light harvesting in red algae. *Plant Physiology* 165(4), 1618–1631 (2014)
- [3] Papáček, Š., Jablonský, J., Matonoha, C., Kaňa, R., Kindermann, S.: FRAP & FLIP: Two sides of the same coin? *Bioinformatics and Biomedical Engineering*, Volume 9044 of the series *Lecture Notes in Computer Science*, 444–455 (2015)
- [4] Axelrod, D., Koppel, D.E., Schlessinger, J., Elson, E., Webb, W.W.: Mobility measurement by analysis of fluorescence photobleaching recovery kinetics. *Biophysical Journal* 16, 1055–1069 (1976)
- [5] Mullineaux, C.W., Tobin, M.J., Jones, G.R.: Mobility of photosynthetic complexes in thylakoid membranes. *Nature* 390, 421–424 (1997)
- [6] Ellenberg, J., Siggia, E.D., Moreira, J.E., Smith, C.L., Presley, J.F., Worman, H.J., Lippincott-Schwartz, J.: Nuclear membrane dynamics and re-assembly in living cells: targeting of an inner nuclear membrane protein in interphase and mitosis. *The Journal of Cell Biology* 138, 1193–1206 (1997)
- [7] Sbalzarini, I.F.: *Analysis, Modeling and Simulation of Diffusion Processes in Cell Biology*. VDM Verlag Dr. Muller (2009)
- [8] Papáček, Š., Kaňa, R., Matonoha, C.: Estimation of diffusivity of phycobilisomes on thylakoid membrane based on spatio-temporal FRAP images. *Mathematical and Computer Modelling* 57, 1907–1912 (2013)
- [9] Kindermann, S., Papáček, Š.: On data space selection and data processing for parameter identification in a reaction-diffusion model based on FRAP experiments. *Abstract and Applied Analysis*, Article ID 859849, 17 pp. (2015)
- [10] Mai, J., Trump, S., Ali, R., Schiltz, R.L., Hager, G., Hanke, T., Lehmann, I., Attinger, S.: Are assumptions about the model type necessary in reaction-diffusion modeling? A FRAP application. *Biophysical Journal* 100(5), 1178–1188 (2011)
- [11] Blumenthal, D., Goldstien, L., Edidin, M., Gheber, L.A.: Universal approach to FRAP analysis of arbitrary bleaching patterns. *Scientific Reports* 5, 11655; doi: 10.1038/srep 11655 (2015)
- [12] Bates, D.M., Watts, D.G.: *Nonlinear regression analysis: Its applications*. John Wiley & Sons, New York (1988)
- [13] Rohn, J., Computing the norm $\|A\|_{\infty,1}$ is NP-hard, *Linear and Multilinear Algebra*, 47, 2000, pp. 195–204.

- [14] Tropp, J., Topics in Sparse Approximation, PhD. Thesis, University of Texas at Austin, 2004.
- [15] Osher S. J., Fedkiw R., Level Set Methods and Dynamic Implicit Surfaces, Springer 2002

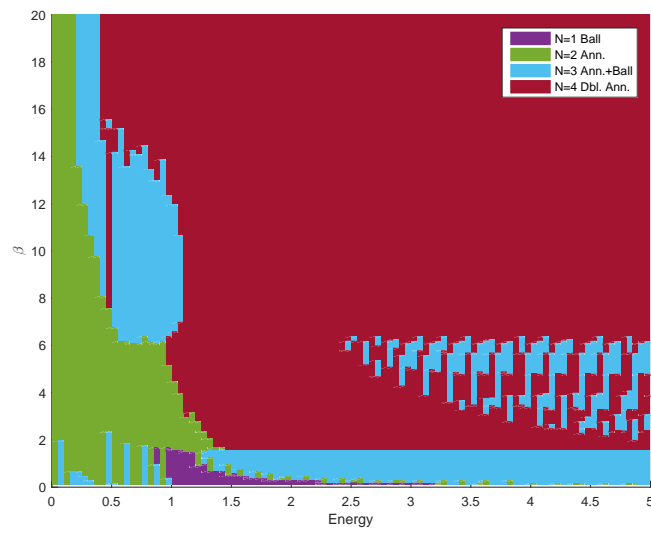


Figure 5: Color-coded illustration of optimal configuration with $N \leq 4$ for different values of β and with fixed values of the energy (Problem 2). The colors indicates which configuration was found optimal.